Journal of Power Sources 245 (2014) 537–542

Contents lists available at SciVerse ScienceDirect

Journal of Power Sources

journal homepage: www.elsevier.com/locate/jpowsour

A new thermal battery for powering borehole equipment: The discharge performance of Li–Mg–B alloy/$LiNO_3$–KNO_3/MnO_2 cells at high temperatures

Yongqiang Niu [a,b], Zhu Wu [a,*], Junlin Du [a,b], Weiyuan Duan [a,b]

[a] Energy Science and Technology Laboratory, Shanghai Institute of Microsystem and Information Technology, Chinese Academy of Sciences, Shanghai 200050, PR China
[b] Graduate School of The Chinese Academy of Sciences, Beijing 100039, PR China

HIGHLIGHTS

- Discharge performance of Li–Mg–B alloy/$LiNO_3$–KNO_3/MnO_2 cells as thermal battery is investigated.
- The discharge mechanism of Li–Mg–B alloy/$LiNO_3$–KNO_3/MnO_2 system is discussed.
- The discharge capacity of Li–Mg–B alloy and MnO_2 in Li–Mg–B alloy/$LiNO_3$–KNO_3/MnO_2 system is determined.
- The new Li–Mg–B alloy/$LiNO_3$–KNO_3/MnO_2 system shows a great potential application in high temperature batteries.

ARTICLE INFO

Article history:
Received 13 January 2013
Received in revised form
24 June 2013
Accepted 25 June 2013
Available online 3 July 2013

Keywords:
Lithium–magnesium–boron alloy
Nitrate electrolyte
Discharge performance
Borehole application

ABSTRACT

There is interest in developing a suitable battery system that can be used at temperatures of 250 °C or less to power instrumentation used in oil/gas and geothermal boreholes. The discharge performance of MnO_2 cathodes with Li–Mg–B alloy anodes is examined using the $LiNO_3$–KNO_3 eutectic electrolyte over a temperature range of 150 °C–300 °C at current densities from 10 to 30 mA cm^{-2}. In this study, we find that the cell can be activated at 150 °C and operate within the desired temperature range without any indication of possible hazards. However, we did observe that temperature and current density significantly affected cell capacity and voltage. Overall, the Li–Mg–B alloy/$LiNO_3$–KNO_3/MnO_2 system shows great potential for powering instrumentation used in oil/gas and geothermal boreholes.

1. Introduction

In recent years, there has been increasing interest in developing a high-temperature battery source that can be used to power the instrumentation used for measurement while drilling (MWD) operations in oil and gas boreholes. In these boreholes, the operating temperatures increase with the depth of the borehole, reaching up to 250 °C. In geothermal boreholes, the operating temperatures can be between 200 °C and 400 °C, which is higher than in oil and gas boreholes. Thermal batteries typically have operating temperatures within the range of 350 °C–600 °C. The temperature within oil/gas and geothermal boreholes is greater than the temperature at which a normal ambient-temperature Li battery operates, but is lower than the operating temperature of a typical thermal battery.

Currently, modified Li–Mg/$SOCl_2$ cells are used to power instrumentation used in deep boreholes made for oil and gas exploration. These cells, manufactured by Battery Engineering, Inc. (Canton, MA), are rated for operation at 180 °C [1]. If these cells were used for powering measurement while drilling equipment in geothermal boreholes, they must be insulated from the immediate thermal environment of boreholes using a metallic vacuum Dewar. However, metallic vacuum Dewars are very expensive and increase the cost of production. If cells were able to function well in the range of 150 °C–300 °C, the temperature of boreholes, then the expensive Dewar system could be avoided.

The melting points of typical electrolytes used in thermal batteries are between 313 °C and 436 °C [2]. An electrolyte having an

* Corresponding author. No. 235, North City Road, Jiading District, Shanghai, PR China. Tel.: +86 21 69976918; fax: +86 21 32200534.
E-mail address: wuzhu@mail.sim.ac.cn (Z. Wu).

0378-7753/$ – see front matter © 2013 Elsevier B.V. All rights reserved.
http://dx.doi.org/10.1016/j.jpowsour.2013.06.140

even lower melting point would be needed for use in oil and gas boreholes, where temperatures reach only around 250 °C [1]. The $LiNO_3$–KNO_3 eutectic electrolyte melts at 124.5 °C and has an ionic conductivity of 0.875 S cm^{-1} at 287 °C, which is promising for oil and gas borehole operations [3]. In addition, this electrolyte is stable at temperatures above 400 °C [4].

The use of high-activity anodes with nitrate electrolytes is only possible because a protective passive oxide film forms on the anode. This film is similar to the film that forms in Li/$SOCl_2$ cells, in which a LiCl film prevents the continued reaction of the Li anode [2]. However, conventional sulfides are not thermodynamically or kinetically stable with molten nitrates and react violently [5]. Miles has performed many studies on the basic electrochemistry of various materials used with the $LiNO_3$–KNO_3 eutectic electrolyte [6]. In his study, it was reported that a Li/$LiNO_3$–KNO_3 battery system combined with a 4-V transition metal oxide cathode material (Ag_2CrO_4 or Ag_3PO_4) significantly increased the energy and power densities of a thermal battery while lowering the operating temperature of the battery by more than 200 °C. Giwa investigated the Li(Al)/Ag_2CrO_4 couple with this electrolyte system, but only over a narrow temperature range of 160 °C–215 °C and at current densities from 10 to 100 mA cm^{-2} [7]. He found that the system was capable of an output of 110 Wh kg^{-1} to a 70% voltage cut-off at 215 °C; current densities up to 100 mA cm^{-2} were achieved. The use of a lithium–boron alloy, developed by the Naval Surface Warfare Center, has a great potential because it contains elemental Li within the pores of the Li–B structure [8]. The use of Li–B anodes in nitrate thermal battery cells was investigated in a study by McManis et al., in which the discharge characteristics of the Li–B alloy anode in molten nitrate electrolytes were examined in the temperature range of 270 °C–350 °C; galvanostatic discharge studies showed no appreciable anode polarization in molten $LiNO_3$ at 300 mA cm^{-2} [9].

The use of Mg as an addition to Li–B alloys to produce ternary alloys has also been reported [10], but electrochemical tests have not yet been conducted. The performance of a Li–Mg–B alloy anode has never been reported when used in a nitrate electrolyte system.

The conventional sulfide electrode materials are not compatible with molten nitrates, so that oxides must be used instead. MnO_2 is chemically compatible with molten nitrate electrolytes at temperatures well over 300 °C [5]. Using MnO_2 as a cathode in molten nitrate electrolyte system is appealing because it is understood to be more environmentally friendly [11].

In this paper, we present the discharge performance of the Li–Mg–B alloy/$LiNO_3$–KNO_3/MnO_2 system. These materials are tested in single cells over a temperature range of 150 °C–300 °C at current densities from 10 to 30 mA cm^{-2}.

2. Experimental

2.1. Materials

The compounds $LiNO_3$ (Analytical Reagent grade) and KNO_3 (Guaranteed Reagent grade) were bought from Sinopharm Chemical Reagent Co. (Shanghai, China). The purity of $LiNO_3$ was ≥99.5%, and the purity of KNO_3 was ≥99.0%. First, $LiNO_3$ and KNO_3 were dried under vacuum for 12 h. Then, the $LiNO_3$–KNO_3 eutectic electrolyte was prepared by fusing the required quantities of components together (33.2% and 66.8%, respectively) in an alumina crucible at 300 °C for 16 h, followed by quenching and grinding (100 mesh). (Unless otherwise noted, all compositions were reported in weight percent.) The separator mixture was prepared by blending the electrolyte powder with 35% MgO, then fusing again at 300 °C for 16 h. The cathode was made up of 70% MnO_2, 10% graphite (as a conductive additive) and 20% electrolyte. The anode was composed of the Li–Mg–B alloy (64%, 4% and 32% respectively, before manufactured). The Li–Mg–B alloy was prepared using the method presented in the United States patent US5,156,806. After manufactured, the amounts of Li and Mg in the Li–Mg–B alloy were found using inductively coupled plasma atomic emission spectroscopy (ICP-AES). The results revealed that the Li–Mg–B alloy contains 60.52% Li and 3.75% Mg. Therefore, the Li–Mg–B alloy was composed of 60.52% Li, 3.75% Mg and 35.73% B. All preparations, processing, and handling of materials and parts were conducted in a glove box under an atmosphere of high-purity argon (<1 ppm each of water and oxygen).

2.2. Single-cell testing

The cathode and separator mixture were cold-pressed into a 15.5 mm in diameter pellet under an applied pressure of 296 MPa. The cathode mass was chosen based on the experiment being performed, and the separator mass was either 0.5 g or 0.3 g. The anode pellet, cut off from the Li–Mg–B alloy sheet, was 19.0 mm in diameter, 0.40 mm thick and weighed 0.097 g. Single cells were discharged under a constant current controlled by a Princeton Applied Research potentiostat/galvanostat (model 273A; Oak Ridge, TN, USA) over a temperature range of 150 °C–300 °C in a glove box under an atmosphere of high-purity argon (<1 ppm each of water and oxygen). Steady-state loads of 10 mA cm^{-2}, 20 mA cm^{-2} and 30 mA cm^{-2} were used. The cell discharge was terminated when the voltage dropped below 1.00 V.

2.3. Thermal analyses

To screen material compatibility and determine the melting points of the $LiNO_3$–KNO_3 eutectic electrolyte, thermal analyses on these materials were conducted by simultaneous differential scanning calorimetry (DSC) and thermogravimetric analysis (TGA) using an STA 449 F3 Jupiter simultaneous thermal analyzer (Netzsch; Boston, MA, USA). These materials are heated to 450 °C at rate of 10 K min^{-1} in an Al_2O_3 pan.

2.4. XRD analysis

To determine the phase composition of the Li–Mg–B alloy, X-ray diffraction measurements were done using a Rigaku D/Max 2200 PC diffractometer (Tokyo, Japan) with CuKα radiation (40 kV, 300 mA, $\lambda = 0.15406$ nm, 4° min^{-1}, $20° \leq 2\theta \leq 90°$). The Li–Mg–B alloy was sealed in a modified glass slide filled with argon gas. All X-ray diffraction measurements were done at room temperature.

3. Results and discussion

3.1. Thermal analyses

Thermal analyses are used to diagnose material compatibility, because this property is essential for the safety of any new high-energy density and high-power density battery system. A number of transition-metal oxides are suitable for use with molten nitrates. The onset temperature for an exothermic reaction between MnO_2 materials and the $LiNO_3$–KNO_3 eutectic electrolyte is around 330 °C [12].

The behavior of the Li–Mg–B anode in the nitrate electrolyte system is examined by simultaneous TGA/DSC, and the results are shown in Fig. 1. From this figure, we find three onset temperatures for endothermic events. The onset of the first endotherm around 115 °C, followed by the major endotherm at 121.3 °C, is likely caused by the impurities in the electrolyte. The onset of the second endotherm around 130 °C, with the major endotherm at 140.4 °C, is resulted from the melting of the electrolyte. This melting temperature is higher than the previously reported melting point of the

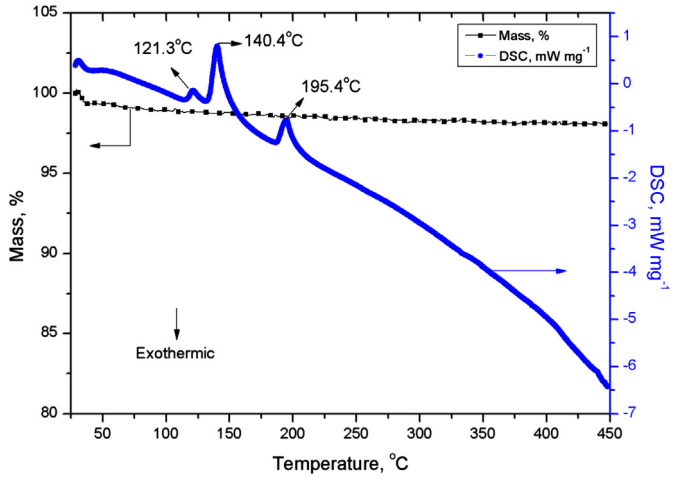

Fig. 1. Simultaneous TGA/DSC responses of the Li–Mg–B alloy with the $LiNO_3$–KNO_3 eutectic electrolyte when heated in argon at 10 K min^{-1}.

$LiNO_3$–KNO_3 eutectic electrolyte, which was found to be 124.5 °C [1]. Another endotherm onset begins around 185 °C, followed by the major endotherm at 195.4 °C, and occurs because the lithium in the Li–Mg–B anode melts. Again, the melting point of Li found in this study is higher than the reported melting point of lithium, 181 °C. The onset temperatures of the second and third endotherms shown in Fig. 1 are both higher than their previously reported values by about 5 °C, which may have occurred because of differences in measurement conditions. Either way, we find no evidence of an exothermic event for temperatures between room temperature and 450 °C.

3.2. X-ray powder diffraction

The XRD pattern reveals information about the bulk structure of the Li–Mg–B alloy. An analysis of the diffraction pattern is presented in Fig. 2. The diffraction peaks in the figure are identified as the characteristic diffraction peaks of Li_5B_4 (JCPDS card no. 43-0878) and Li_3Mg_7 (JCPDS card no. 65-6742). Because the reference pattern of LiB (JCPDS card no. 52-1033) is similar to that of Li_5B_4, it is very difficult to determine if LiB exists in the alloy because of the superposition of peaks. However, a diffraction peak around 42° is present in the XRD pattern that is also seen in the LiB pattern, but the peak is not present in the Li_5B_4 pattern. Therefore, it is our conjecture that LiB also exists in the Li–Mg–B alloy.

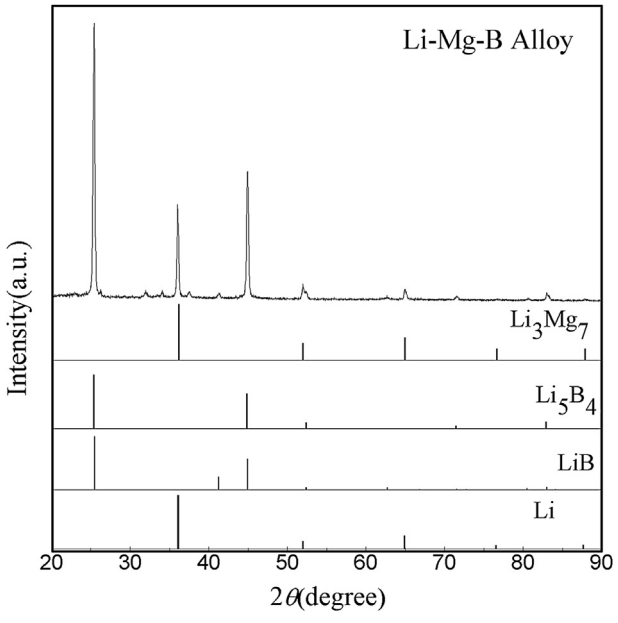

Fig. 2. Evolution of the X-ray diffraction patterns of the Li–Mg–B alloy, which is done using a Rigaku D/Max 2200 PC diffractometer with CuKα radiation (40 kV, 300 mA, $\lambda = 0.15406$ nm, 4° min^{-1}, $20° \leq 2\theta \leq 90°$).

Although the phase of Li (JCPDS card no. 15-0401) cannot be clearly seen in the diffraction pattern of the Li–Mg–B alloy, it is our conjecture that Li also exists in the Li–Mg–B alloy. There are several reasons for this conjecture: First, the Li–Mg–B alloy is susceptible to air oxidation; Second, the TGA/DSC results (the endotherm onset begins around 185 °C, followed by the major endotherm at 195.4 °C) show that Li exists in the alloy; Last, it has been previously reported that lithium–boron alloy contains elemental Li within the pores of the Li–B structure [8], and the Li–Mg–B alloy is a ternary alloys which is similar with Li–B alloy.

3.3. Single-cell tests

In this paper, we surmise that the Li–Mg–B alloy is composed of Li_5B_4, Li, LiB and Li_3Mg_7.

The $Li_aMg_bB_c$ alloy, where a, b, and c are the weight percentages of Li, Mg, and B, respectively, contains $w_1Li_5B_4$, w_2Li, w_3LiB, and $w_4Li_3Mg_7$, where w_1, w_2, w_3, and w_4 are the weight percentages of Li_5B_4, Li, LiB, and Li_3Mg_7, respectively. We then obtain the following equations:

$$a + b + c = 100 \quad (1)$$

$$w_1 + w_2 + w_3 + w_4 = 100 \quad (2)$$

$$0.445w_1 + w_2 + 0.391w_3 + 0.109w_4 = a \quad (3)$$

$$0.891w_4 = b \quad (4)$$

$$0.555w_1 + 0.609w_3 = c \quad (5)$$

Solving the system of equations, we find:

$$w_1 = 1.2017c,\ w_2 = a - 0.1224b - 0.7490c,\ w_3 = 0.5473c,\ w_4 = 1.1224b$$

From these calculations, we find that the Li–Mg–B alloy consists of 42.94% Li_5B_4, 33.30% Li, 19.55% LiB and 4.21% Li_3Mg_7. Because the Li–Mg–B alloy actually contains Li and Li_3Mg_7 in the pores of the Li–B structure formed by LiB and Li_5B_4, the theoretical capacity of the Li–Mg–B alloy is calculated to be 1386.3 mAh g^{-1}.

Fig. 3 shows the effect of temperature on the performance of Li–Mg–B alloy/$LiNO_3$–KNO_3/MnO_2 cells discharged at 10 mA cm^{-2} when a 0.50 g cathode, a 0.097 g anode pellet, and a 0.50 g separator are used. Three distinct discharge plateaus are evident during discharge (2.90 V, 2.70 V, and 2.10 V, respectively), and a fourth plateau (1.50 V) is found in cells discharged at 200 °C and 250 °C. The performance of Li–Mg–B alloy/$LiNO_3$–KNO_3/MnO_2 single cells is excellent at 200 °C and 250 °C. However, at 150 °C, there is a large drop in voltage and capacity, which is primarily caused by the poor electrolyte kinetics (low ionic conductivity) evident at lower temperatures. At 300 °C, there is another large drop in voltage and capacity. This drop most likely reflects the heightened self-discharge in the system, which is generally caused by the increased activities of the anode and cathode at higher temperatures.

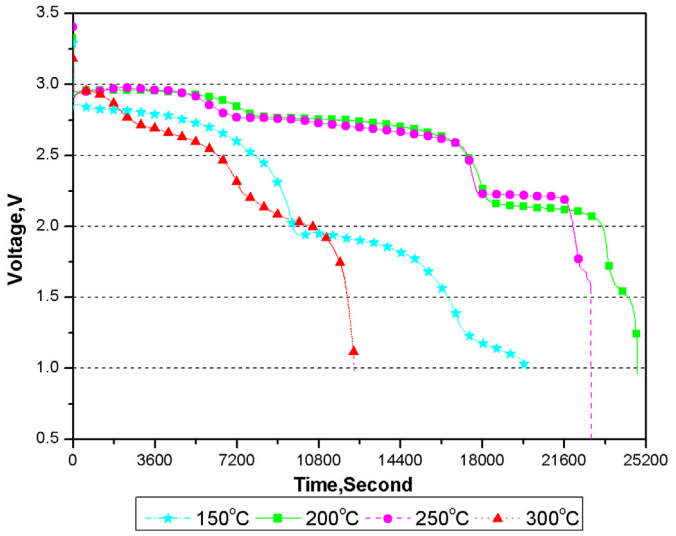

Fig. 3. The effect of temperature on the performance of Li–Mg–B alloy/$LiNO_3$–KNO_3/MnO_2 single cells discharged at 10 mA cm^{-2} when a 0.50 g cathode, a 0.097 g anode pellet, and a 0.50 g separator are used.

To determine the discharge capacity of the Li–Mg–B alloy, cathodes having different mass are used. Fig. 4 shows the performance of Li–Mg–B alloy/$LiNO_3$–KNO_3/MnO_2 single cells at 200 °C and a current density of 10 mA cm^{-2} when different mass of cathodes, a 0.5 g separator, and a 0.097 g anode are used. The relative capacities of the cells are 130.90 mAh and 131.60 mAh (almost equal) before the cells discharges are terminated. This finding suggests that a 0.5 g cathode is in excess relative to the 0.097 g Li–Mg–B anode. The capacity of the 0.097 g Li–Mg–B alloy is 131.60 mAh before the cells discharge are terminated. So, the capacity of the Li–Mg–B alloy is 1356.7 mAh g^{-1}, which is close to its theoretical value of 1386.3 mAh g^{-1}. In this situation, we believe that the Li_3Mg_7 component of the Li–Mg–B alloy is involved in the discharge reaction. The capacities and plateau voltages for different Li-alloy anodes found by Guidotti and Masset [13] are presented in Table 1. From this table, we find that the capacity of the Li–Mg–B alloy is larger than most other Li-alloy anodes.

Table 1
Capacities and plateau voltages for candidate Li-alloy anodes.

Anode	Capacity ($mAhg^{-1}$)	Capacity ($mAhcm^{-3}$)	Discharge emf/mV vs. Li^0 (T/°C)
Li in LAN (20 w/o Li)	772.5	1613.3	0
Li in Ni wick (17% dense)	838.6	1637.8	0
Li–Al (20 w/o Li)	627.5	1091.9	297(415)
$Li_{13}Si_4$ (44 w/o Li) (1st transition)	485.3	669.7	157(415)
Mg_2Si–Mg–$Li_{13}Si_4$	876.4	>1209.4	60(415)
Li–B (70 w/o Li)	1333.3	1083.3	20(500)
Li–B (80 w/o Li)	2138.9	1500.0	20(500)
$Li_{10}Si_2B$ (50.9w/oLi) (1st transition)	393.1	–[a]	50(400)
Li_8Si_2B (45.3w/oLi) (1st transition)	503.1	800.0	157(400)
Li_7Sn_3(12 w/o Li)(1st transition)	265.0	–[a]	450(415)
Li_9Ge_4 (17.7 w/o Li)(1st transition)	380	950.0(est.)	420(400)
$Li_{16}Ge_5$ (23.4 w/o Li)(1st transition)	268.6	671.7(est.)	236(400)

[a] Density value needed for calculation not available.

In order to work out the reaction mechanism, different mass of cathodes are used. Fig. 5 shows the performance of Li–Mg–B alloy/$LiNO_3$–KNO_3/MnO_2 single cells discharged at 10 mA cm^{-2} when 0.50 g, 0.75 g, 1.00 g, or 1.50 g cathodes are used.

Based on the relationship between the discharge time and the amount of cathode used, we infer the reactions of the various plateaus [14].

At the first plateau, the cathode reaction is

$$2MnO_2 + 0.8Li^+ + 0.8e \rightarrow Li_{0.8}Mn_2O_4 \quad (6)$$

and the anode reaction is

$$0.8Li \rightarrow 0.8Li^+ + 0.8e \quad (7)$$

At the second plateau, the cathode reaction is

$$Li_{0.8}Mn_2O_4 + 1.2Li^+ + 1.2e \rightarrow Li_2Mn_2O_4 \quad (8)$$

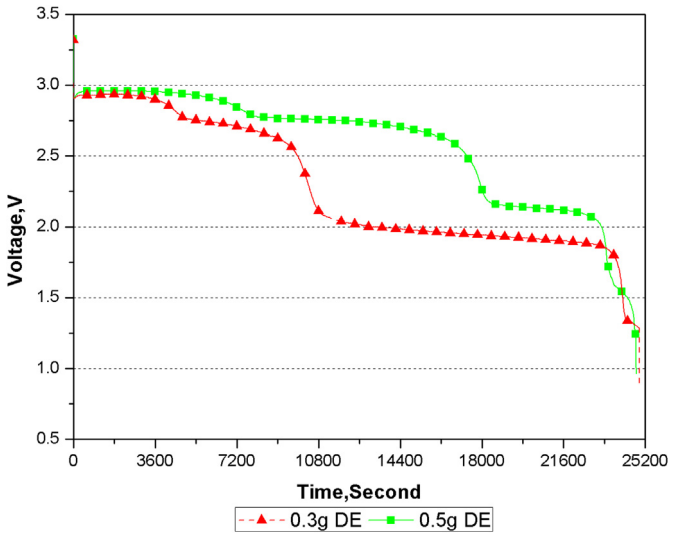

Fig. 4. The performance of Li–Mg–B alloy/$LiNO_3$–KNO_3/MnO_2 single cells discharged at 200 °C and a current density of 10 mA cm^{-2} when different mass of cathodes are used with a 0.5 g separator and a 0.097 g Li–Mg–B anode.

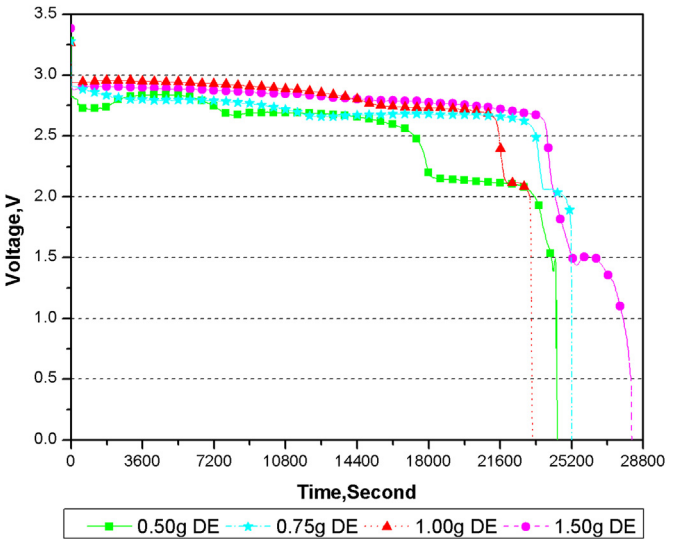

Fig. 5. The performance of Li–Mg–B alloy/$LiNO_3$–KNO_3/MnO_2 single cells discharged at 10 mA cm^{-2} when 0.50 g, 0.75 g, 1.00 g, or 1.50 g cathodes are used with a 0.3 g separator and a 0.097-g Li–Mg–B anode.

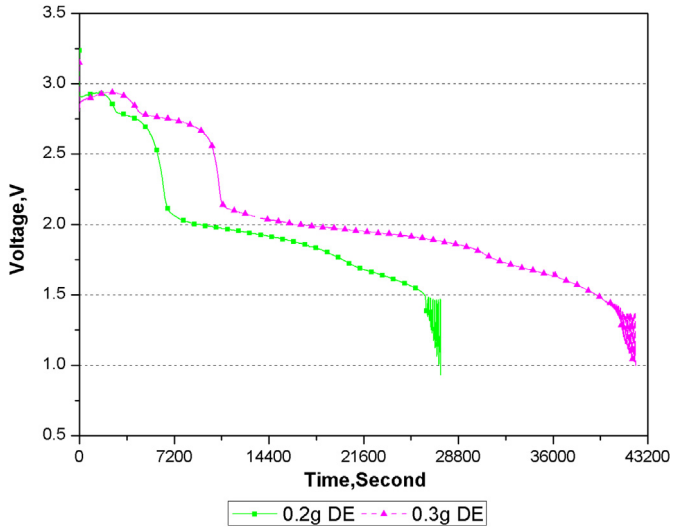

Fig. 6. The performance of Li–Mg–B alloy/$LiNO_3$–KNO_3/MnO_2 single cells discharged at a temperature of 200 °C and a current density of 10 mA cm^{-2} when 0.2 g or 0.3 g cathode are used with a 0.3 g separator and double Li–Mg–B pellets anode.

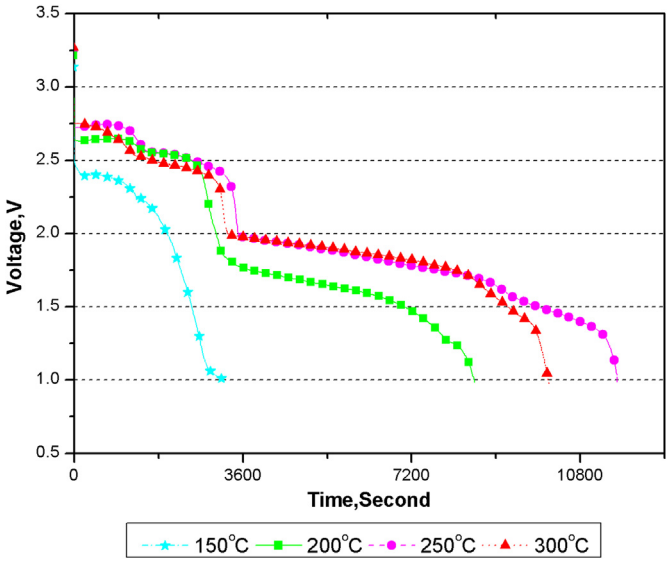

Fig. 7. Effect of temperature on the performance of Li–Mg–B alloy/$LiNO_3$–KNO_3/MnO_2 single cells discharged at 20 mA cm^{-2}.

and the anode reaction is

$$1.2Li \rightarrow 1.2Li^{+} + 1.2e \quad (9)$$

At the third plateau, the cathode reaction is

$$Li_2Mn_2O_4 + 4Li^{+} + 3NO_3^{1-} + 4e \rightarrow 2Li_2MnO_3 + 3NO_2^{1-} + Li_2O \quad (10)$$

and the anode reaction is

$$4Li \rightarrow 4Li^{+} + 4e \quad (11)$$

At the fourth plateau, the cathode reaction is

$$Li_{0.8}Mn_2O_4 + 3xLi^{+} + 7xMg^{2+} + 17xe \rightarrow Li_{0.8+3x}Mg_{7x}Mn_2O_4 \quad (12)$$

(where x is a trace variable) and the anode reaction is

$$xLi_3Mg_7 \rightarrow 3xLi^{+} + 7xMg^{2+} + 17xe \quad (13)$$

MnO_2 is believed to involve reaction of Formula (a). The theoretical capacity of MnO_2 is calculated to be 924.9 mAh g^{-1}.

$$MnO_2 \rightarrow Li_{0.8}Mn_2O_4 \rightarrow Li_2Mn_2O_4 \rightarrow Li_2MnO_3 \quad (a)$$

To determine the discharge capacity of MnO_2, double Li–Mg–B pellets are used. Fig. 6 shows the performance of Li–Mg–B alloy/$LiNO_3$–KNO_3/MnO_2 single cells at 200 °C and a current density of 10 mA cm^{-2} when 0.2 g, 0.3 g cathode are used with a 0.3 g separator and double Li–Mg–B pellets anode.

The relative capacities of the cells are found to be 145.04 mAh and 223.15 mAh before the cells discharges are terminated. The capacity doesn't increase in proportion with the anode mass—the capacity of double Li–Mg–B pellets should be about 260 mAh—and the discharged anode shows that the double Li–Mg–B alloy pellets are in excess. The capacity of the cathode, which contains 70% MnO_2, is around 736.38 mAh g^{-1}. So, the capacity of MnO_2 is found to be 1052.0 mAh g^{-1}, which is larger than the theoretical value of 924.9 mAh g^{-1}. This anomalous likely resulted from the reduction of Li_2MnO_3 to $Li_{2+y}Mn_2O_4$ (where y is a trace variable).

To maintain an equal capacity, a 0.1787 g cathode must be used with the 0.097 g Li–Mg–B alloy. Due to the lower cost of MnO_2 compared to the anode components, we determine that increasing the amount of the cathode is the most economical choice. Therefore, a 0.097 g Li–Mg–B alloy, a 0.3 g separator and a 0.2 g cathode are used to test the cell at different current densities and different temperatures.

Similar data for current densities of 20 mA cm^{-2} and 30 mA cm^{-2} are presented in Figs. 7 and 8, respectively. The performance of these cells shows degraded discharge characteristics (large drop in voltage, less voltage plateaus) at the higher current density. This is probably caused by several factors: the electrolyte can't afford the abundant Li^{+} ions when the cells are discharged at the higher current density at 150 °C–300 °C; polarization is probably caused by the precipitation of Li_2O, which blocks the active sites at the anode [15]; the conductivities of the cathode and anode can't afford the higher current density at 150 °C–300 °C.

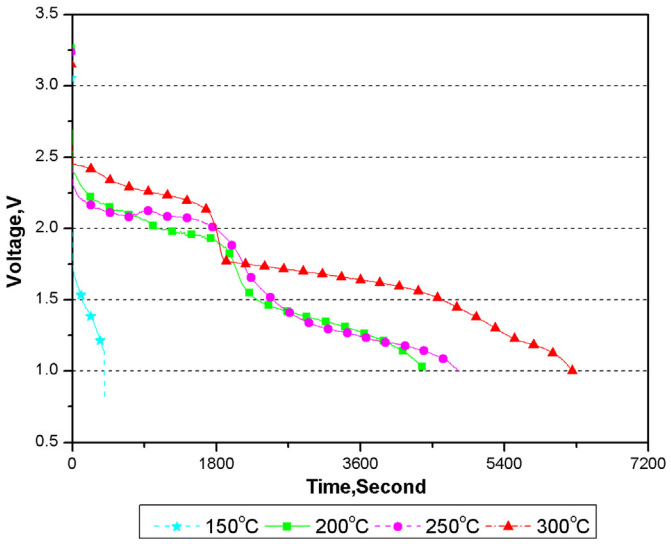

Fig. 8. Effect of temperature on the performance of Li–Mg–B alloy/$LiNO_3$–KNO_3/MnO_2single cells discharged at 30 mA cm^{-2}.

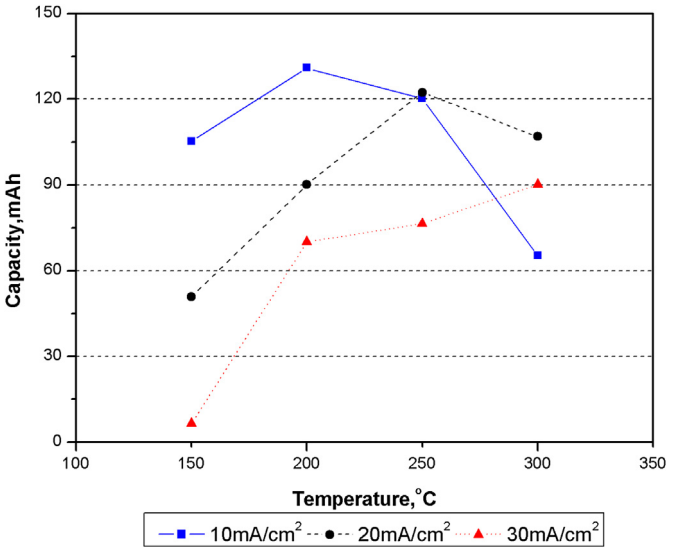

Fig. 9. Effect of temperature and current density on the discharge capacities of Li–Mg–B alloy/$LiNO_3$–KNO_3/MnO_2 single cells discharged at 10, 20, and 30 mA cm^{-2}.

Fig. 7 shows that the performance of the cell discharged at 250 °C was optimal when the current density is 20 mA cm^{-2}, while Fig. 8 shows that the performance of the cell discharged at 300 °C is optimal when the current density is 30 mA cm^{-2}. This finding reflects that when the temperature is elevated, battery performance will be improved under a high steady load.

There are several factors, including discharge rate, temperature, and cell thickness, that affect a cell's lifetime [16]. The effects of temperature and current density on the capacity of the cell are summarized in Fig. 9. We find that at higher temperatures, there is a competition between capacity losses due to self-discharge and capacity increases due to improved kinetics. When cells are discharged at a current density of 10 mA cm^{-2}, the cell's capacity shows a maximum value near 200 °C, followed by a monotonic decrease in capacity as the temperature increases. When cells are discharged at a current density of 30 mA cm^{-2}, the cell's capacity shows a monotonic increase as the temperature increases. When cells are discharged at the same temperature, a decreasing trend in cell capacity is observed as the current density increases. These findings suggest that elevating the temperature can increase the cell's capacity when the cell is discharged at high current density.

4. Conclusions

Our investigation of the behavior of the Li–Mg–B alloy anode used in conjunction with the $LiNO_3$–KNO_3 electrolyte system does not reveal any significant hazards for operation in the temperature range consisting of room temperature to 450 °C.

Analysis of the diffraction pattern of the Li–Mg–B alloy suggests that the Li_5B_4 and Li_3Mg_7 phases exist in the alloy. In addition, we find that the Li–Mg–B alloy/$LiNO_3$–KNO_3/MnO_2 thermal battery cell can be activated at 150 °C and operated over a temperature range of 150 °C–300 °C to produce 3.1–3.4 V at open–circuit and initial operating voltages above 2.90 V at 10 mA cm^{-2}. In this system, the capacity of the Li–Mg–B alloy is 1356.7 mAh g^{-1}, and the capacity of MnO_2 is found to be 1052.0 mAh g^{-1}. However, both temperature and current density hugely affected cell capacity. At the same temperature, cell capacity decreases with increasing current density.

The discharge mechanism of the Li–Mg–B alloy/$LiNO_3$–KNO_3/MnO_2 system is also investigated; MnO_2 is believed to be involved in the reaction of from MnO_2 to $Li_{0.8}Mn_2O_4$, then to $Li_2Mn_2O_4$, and last to Li_2MnO_3.

We find that the Li–Mg–B alloy/$LiNO_3$–KNO_3/MnO_2 system could be used at temperatures of 250 °C or below to power instrumentation used in geothermal and oil/gas boreholes fields. However, this system has some specific restrictions associated with temperature and discharge rate.

Acknowledgments

Energy Science and Technology Laboratory is a new energy research center operated by the Shanghai Institute of Microsystem and Information Technology, Chinese Academy of Science, under the Scientific Research Project of Science and Technology Commission of Shanghai Municipality (09dz1206800).

Appendix A. Supplementary data

Supplementary data related to this article can be found at http://dx.doi.org/10.1016/j.jpowsour.2013.06.140.

References

[1] R.A. Guidotti, 35th Intersociety Energy Conversion Engineering Conference and Exhibit (IECEC), Amer Inst Aeronautics & Astronautics, Reston, 2000.
[2] R.A. Guidotti, F.W. Reinhardt, Performance of Li–alloy/Ag_2CrO_4 Couples in Molten $LiNO_3$–KNO_3 Eutectic Electrolyte, Electrochemical Society Inc, Pennington, 2002.
[3] R.A. Guidotti, P.J. Masset, Primary Batteries – Reserve Systems|Thermally Activated Batteries: Lithium, in: G. Jürgen (Editor-in-Chief), Encyclopedia of Electrochemical Power Sources, Elsevier, Amsterdam, 2009, pp. 141–155.
[4] G.E. McManis, M.H. Miles, A.N. Fletcher, J. Power Sources 16 (1985) 243–251.
[5] P. Masset, R.A. Guidotti, J. Power Sources 164 (2007) 397–414.
[6] M.H. Miles, in: Battery Conference on Applications and Advances, 1999 (1999), pp. 39–42. The Fourteenth Annual.
[7] C.O. Giwa, Feasibility Study of Materials for a Medium–temperature Reserve Cell Concept, Trans Tech Publications Ltd, Zurich, 1991.
[8] R. Szwarc, R.D. Walton, S. Dallek, B.F. Larrick, J. Electrochem. Soc. 129 (1982) 1168–1173.
[9] G.E. McManis, M.H. Miles, A.N. Fletcher, J. Electrochem. Soc. 131 (1984) 286–289.
[10] R.A. Sutula, F.E. Wang, U.S. Patent 5,156,806, May 5, 1975.
[11] P.J. Masset, R.A. Guidotti, J. Power Sources 178 (2008) 456–466.
[12] R.A. Guidotti, F.W. Reinhardt, J. Odinek, J. Power Sources 136 (2004) 257–262.
[13] R.A. Guidotti, P.J. Masset, J. Power Sources 183 (2008) 388–398.
[14] Yongqiang Niu, Zhu Wu, Junlin Du, J. Electrochem. Soc. 160 (2013) A1375–A1379.
[15] M.H. Miles, A.N. Fletcher, J. Appl. Electrochem. 10 (1980) 251–260.
[16] G.E. McManis, A.N. Fletcher, M.H. Miles, J. Appl. Electrochem. 16 (1986) 636–642.